How to cite: *Angew. Chem. Int. Ed.* **2022,** *61,* e202207559
International Edition: doi.org/10.1002/anie.202207559
German Edition: doi.org/10.1002/ange.202207559

VIP **3D COF Membranes** *Very Important Paper*

Design of Three-Dimensional Covalent Organic Framework Membranes for Fast and Robust Organic Solvent Nanofiltration

*Xiansong Shi, Zhipeng Zhang, Congcong Yin, Xin Zhang, Jianghai Long, Zhe Zhang, and Yong Wang**

Abstract: Organic solvent nanofiltration (OSN) has become increasingly important in petrochemical and pharmaceutical industries, demanding superior and robust membranes. Herein, we report advanced OSN processes by designing three-dimensional covalent organic framework (3D COF) membranes through moderated interfacial crystallization. Nanoporous supports work as the moderator allowing the crystallization of 3D COF membranes. The 3D COF features sub-nanometer and anti-swelling channels, affording a sharp selectivity to fine targets with an exceptionally high and stable methanol permeance. Thus-synthesized membrane exhibits a record stability against high-concentration feeds and long-term operation for ≈1000 h. Moreover, we unambiguously demonstrate that our membrane holds excellent practicality in purifying active pharmaceutical ingredients from organic liquids. This work reveals the great potential of distinctive 3D COFs in producing prominent OSN membranes for industrial applications.

Introduction

Organic liquids are deemed to be indispensable in advancing petroleum, chemical, and pharmaceutical industries. Especially in the manufacturing of active pharmaceutical ingredients (APIs), more than 80 % of the material consumption can be assigned to the usage of organic solvents.[1] While high-tech means are rising to lessen the solvent expenditure, the worldwide necessity for organic solvents is inexorably growing.[2] This motivates the exploitation of novel strategies to recycle solvents on one hand, and the development of robust materials with sustained stability and performance on the other hand.[3] In this context, membrane-based separations have become a promising technology because of their eco-friendly process, low energy consumption, and small carbon footprints.[4] In particular, organic solvent nanofiltration (OSN) can spare about 90 % energy expenditure, compared with those energy-intensive thermal processes.[5] More importantly, OSN techniques require mild operational conditions having a negligible influence on the product activity, making them an ideal platform to recover and upgrade environmentally sensitive biomolecules.[6]

Experimental and theoretical studies on exploring reliable OSN processes have received great successes.[7] However, hampered by deficient porosities and dispersive pore sizes, achieving fast but selective separation of fine molecules by traditional OSN membranes remains challenging.[6] To practically meet these strict separation demands, OSN membranes should be provided with the prerequisites including small, ordered channels, high pore connectivity, and structural robustness. Since building materials are regarded as the cornerstone of OSN membranes, their development and innovation play a decisive role in promoting overall performances. Currently, a variety of organic, inorganic, and hybrid materials have been developed to build viable OSN membranes.[8] Aside from the prevailing polyamide (PA) and its derivatives, polymers with intrinsic microporosity (PIMs),[9] conjugated microporous polymers (CMPs),[10] and two-dimensional (2D) materials[11] have emerged as nascent building blocks. Nevertheless, membranes composed of these conventional materials can barely meet the criteria mentioned before, which involve suboptimal pore uniformity and notorious swelling issues, making them inadequate for fine and durable separations. It is incontestable that the inborn drawbacks of those materials can be partially addressed by complex modifications,[12] whereas the serious permeability and selectivity trade-off remains. Moreover, the majority of studies on OSN membranes simply adopt dye molecules as the probe to assess performances, lacking a practical demonstration. Thus, exploiting novel materials which could completely satisfy the stringent criteria and revealing their practicality in advanced OSN processes are tremendously desired.

Covalent organic frameworks (COFs), featuring tailorable and predictable structures, have been regarded as a burgeoning candidate to revolutionize membrane materials and technologies.[13] The neat COF membranes reported in 2017 represents a breakthrough in the application of COFs toward aqueous separation.[14] In contrast, the development of COF membranes toward organic liquids is still in the infancy stage.[15] Additionally, the feasibility of COF membranes in separating fine molecules (molecular weight < 350 Da) from organic solvents remains to be explored. We reason that COF materials are greatly competitive for treating organic liquids by exerting their excellent solvent resistance and phenyl-enriched hydrophobic skeletons. Moreover, the crystalline nature of COFs could promise

[*] X. Shi, Z. Zhang, C. Yin, X. Zhang, J. Long, Y. Wang
State Key Laboratory of Materials-Oriented Chemical Engineering, College of Chemical Engineering, Nanjing Tech University
Nanjing 211816, Jiangsu (P. R. China)
E-mail: yongwang@njtech.edu.cn

robust structures without deformability in aggressive solvents, rendering a long-standing selectivity that exclusively depends on the invariable aperture size. The elaborate design of COFs by reticular chemistry and polymer science further promises the on-demand membrane preparation at the atomic/molecular level for specific separations.[16] However, COF membranes are prevailingly constructed by 2D COFs featuring large apertures and limited pore connectivity,[17] thus showing an inefficiency for highly permselective OSN. Three-dimensional (3D) COFs, as a subset of COF family, are inherently equipped with ultrafine apertures and remarkable pore connectivity, in favor of upgrading selectivity and permeability simultaneously. Therefore, by virtue of their unique characteristics, 3D COFs could afford enormous potentials to innovate OSN membranes with precisely tailored structures and significantly improved performances.

Herein, we introduce a feasible method to produce highly permselective and robust OSN membranes through the topological design of a 3D COF. The anti-swelling 3D COF with interpenetrated sub-nanometer channels is rationally devised as the molecular sieving layer by a strategy of moderated interfacial crystallization. We systematically perform the synthetic and structural characterizations of the 3D COF and its OSN performances. The specifically designed channels offer a fast and exclusive permeation of organic solvents, which results in remarkable permselectivity outperforming state-of-the-art OSN membranes. The feasibility of our membranes in durable OSN process and pharmaceutical engineering is distinctly demonstrated, showing their huge practicality in industrial applications.

Results and Discussion

Upgrading the selectivity of OSN membranes by deficient methods could deteriorate their permeability, and *vice versa*.[18] In this work, to reconcile a sharp selectivity and high permeability, we targeted the synthesis of subnanoporous 3D COFs with high pore penetrability. Distinct from existing 2D COF membranes, the ultrafine but interpenetrated channels of 3D COFs could generate a notable promotion on selectivity without compromising permeability due to the abundant mass transfer paths.[19] Specifically, TFPM-HZ is devised and synthesized through the condensation between tetrakis(4-formylphenyl)-methane (TFPM) and hydrazine hydrate (HZ) under solvothermal conditions (Figure 1a). The tetrahedral node ensures an accurate 3D geometrical framework,[20] while the short linker benefits for producing sub-nanometer channels (Figure 1b). Here, the

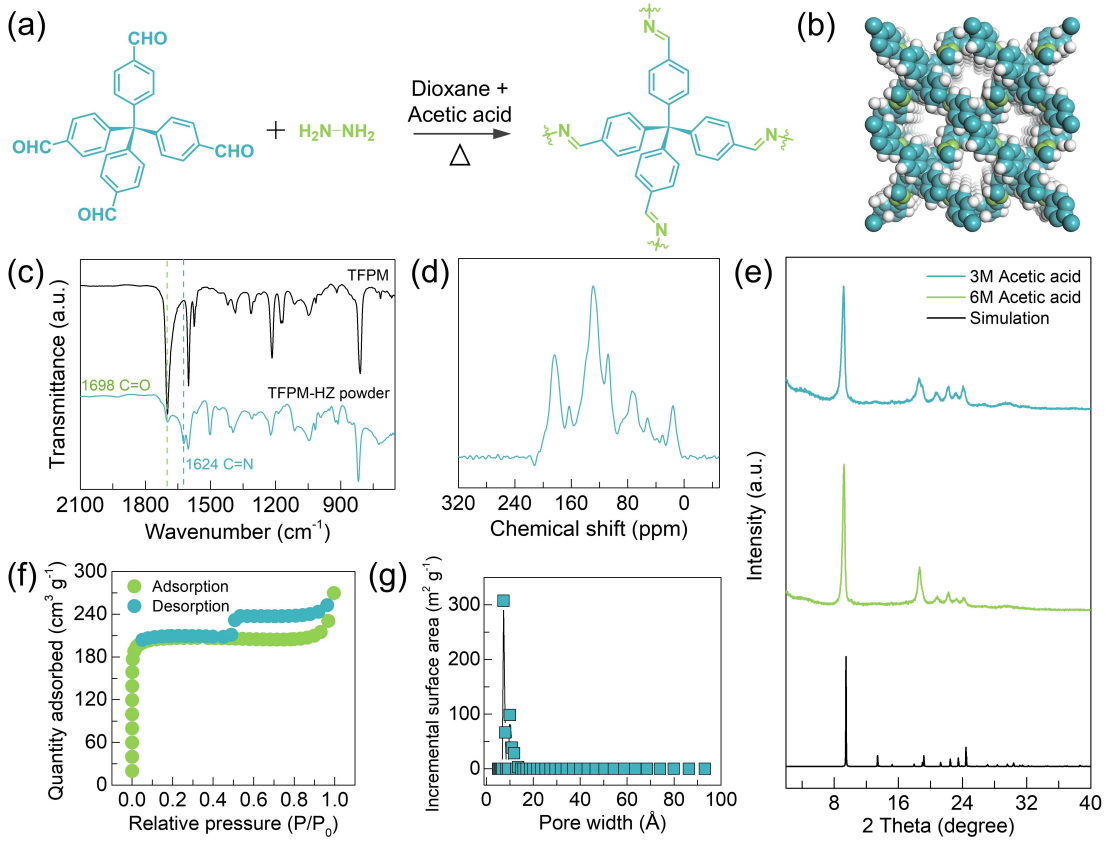

Figure 1. Synthesis and characterization of TFPM-HZ. a) Schematic diagram for the synthesis of TFPM-HZ. b) Molecular structure of TFPM-HZ. c) FTIR spectra of TFPM-HZ and TFPM. d) ^{13}C solid-state NMR spectrum of TFPM-HZ. e) Experimental and simulated PXRD patterns of TFPM-HZ. f,g) Nitrogen adsorption-desorption isotherms of the TFPM-HZ powder and the corresponding pore size distribution. Dash lines in (c) indicate the position of characteristic peaks.

formation of imine linkages follows the dynamic covalent chemistry, which is perceived as contributing to forming highly crystalline COFs by virtue of reversible error correction.[21] After reaction and purification, light yellow precipitates showing a spherical morphology with sizes of ≈500 to 1000 nm are obtained (Figure S1). As probed by Fourier transform infrared spectroscopy (FTIR), the intensity of the C=O stretching vibration at ≈1698 cm^{-1}, assigned to TFPM, is notably diminished (Figure 1c). This indicates the occurrence of the condensation reaction. Moreover, the resulting precipitates exhibit a new vibration at ≈1624 cm^{-1}, suggesting the formation of imine bonds.[22] ^{13}C solid-state nuclear magnetic resonance (NMR) spectroscopy further confirms the characteristic signal of C=N bonds at ≈162 ppm (Figure 1d). Structural determination by powder X-ray diffraction (PXRD) validates conspicuous crystallinity of TFPM-HZ, visualized by the diffraction peaks at 2θ values of 9.3, 18.6, 20.7, 22.3, and 24.1° (Figure 1e).[23] The intense peaks of TFPM-HZ produced by 3 M and 6 M acetic acid as the catalyst verify the excellent reproducibility of this work. More importantly, the crystalline framework is essentially retained after being treated in various solvents (Figure S2). Figure 1f shows the nitrogen adsorption-desorption isotherms at 77 K and we can observe a sharp gas uptake at low relative pressures, identifying the microporous nature of TFPM-HZ. The hysteresis loop of isotherms in the 0.5–1.0 P/P_0 range suggests the presence of textural mesopores possibly raising from the agglomeration of TFPM-HZ crystals.[24] The Brunauer–Emmett–Teller (BET) surface area of TFPM-HZ is determined to be ≈626 $m^2 g^{-1}$. Fitting nonlocal density functional theory identifies a sharp pore width distribution centered at 0.75 nm (Figure 1g), in accordance with the subnanopores predicted from the structure. This aperture size adequately allows solvent transport while rejecting small solutes with sizes >0.8 nm, making TFPM-HZ particularly suitable for building high-performance OSN membranes. Thermogravimetric analysis (TGA) reveals that TFPM-HZ is thermally stable at the temperature of up to 325 °C in nitrogen atmosphere (Figure S3). With these complementary results, we conclude that the condensation of TFPM and HZ generates a highly crystalline 3D COF featuring uniformly interpenetrated, sub-nanometer channels.

With the success in TFPM-HZ synthesis, we then focused on the exploration of a viable strategy to fabricate its membrane for separations. Although those crystalline COF membranes by solvothermal growth,[16a,25] a method to crystalize COFs at mild conditions affords the feasibility to produce their large-area membranes. In view of its high activity to mediate imine formation and transamination, scandium trifluoromethane sulfonate ($Sc(CF_3SO_3)_3$) was selected as a novel catalyst to promote the crystallization of TFPM-HZ under ambient conditions.[26] TFPM-HZ synthesized at room temperature exhibits the diffraction peaks and nitrogen adsorption-desorption isotherms matching well with the solvothermal counterpart, indicative of the similar crystalline framework (Figure S4–S5). The molecular sieving layer built of TFPM-HZ was synthesized on porous polyacrylonitrile (PAN) supports to produce composite membranes (designated as TFPM-HZ/PAN) by moderated interfacial crystallization (Figure 2a). Specifically, the monomer pairs dispersed in ethyl acetate and $Sc(CF_3SO_3)_3$ dissolved in water served as the organic and aqueous phases, respectively. A key aspect of this strategy is introducing a nanoporous support at the designed organic-aqueous interface. As previously reported by Tan *et al*,[27] the reaction rate plays a decisive role in forming crystalline covalent triazine frameworks. Here, the PAN support acts as a moderator, allowing the controlled diffusion of $Sc(CF_3SO_3)_3$ from water to ethyl acetate (Figure S6), thus reducing the reaction rate to form crystalline TFPM-HZ. It is noteworthy that no polymerization occurs in the absence of $Sc(CF_3SO_3)_3$ (Figure S7), revealing its high-efficiency catalysis. A synthesis duration of 36 h can generate compact and dense TFPM-HZ/PAN membranes without any defects or pinholes (Figure 2b, Figure S8). Morphological and structural features of thus-obtained membranes were thoroughly characterized. Taking the membrane synthesized for 48 h as an example, it exhibits a shiny appearance, in sharp contrast to the lackluster PAN support (Figure 2c, Figure S9). Atomic force microscopy (AFM) reveals an extremely smooth membrane surface, showing a low roughness of ≈1.5 nm (Figure 2d). The cross-sectional SEM image presents a continuous TFPM-HZ layer firmly attached to the support, and the top thickness of TFPM-HZ is estimated to be ≈70 nm (Figure 2e, Figure S10). Thanks to the polymeric nature of COFs, the flexible support grown with TFPM-HZ sustains high flexibility and exhibits the effect of thin film interference (Figure S11). To obtain better insights into the structure of the TFPM-HZ layer, it was detached from the support by immersing in N, N-dimethylformamide (DMF) (Figure S12a–b). With the dissolution of PAN, we thus obtained self-supporting TFPM-HZ (designated as s-TFPM-HZ) membranes. The s-TFPM-HZ membranes are highly flexible and robust in area of over 12 cm^2, and no breakages and cracks are observed. Figure 2f illustrates the s-TFPM-HZ membrane transferred to a metal lasso, which presents an intact surface covering the entire lasso, hinting at the excellent mechanical strength.[28] Benefiting from the robust skeleton and physical flexibility, the s-TFPM-HZ membrane retains the structural integrality when pumped by a pipette, enabling the collection of s-TFPM-HZ membranes into a glass vessel (Movie S1, Figure S12c). As a contrast, the TFPM-HZ membrane crystalized at the support-free interface is prone to fracture during transferring (Figure S13), providing the evidence for the support-regulated crystallization. Interestingly, the SEM and transmission electron microscopy (TEM) studies disclose a rough bottom surface with perforated structures (Figure 2g, Figure S14), distinctive from the compact top surface. We attribute this asymmetrical architecture to the embedded growth of TFPM-HZ in the porous PAN skin layer, as confirmed by the large entire thickness, which is nearly three times higher than the previously estimated top thickness (Figure 2h,i). The slight solubility of ethyl acetate in water is ultimately responsible for this microstructure. In this case, the TFPM-HZ layer tightly interlaces with the PAN support, thus forming a mechanically stable composite structure superior to the

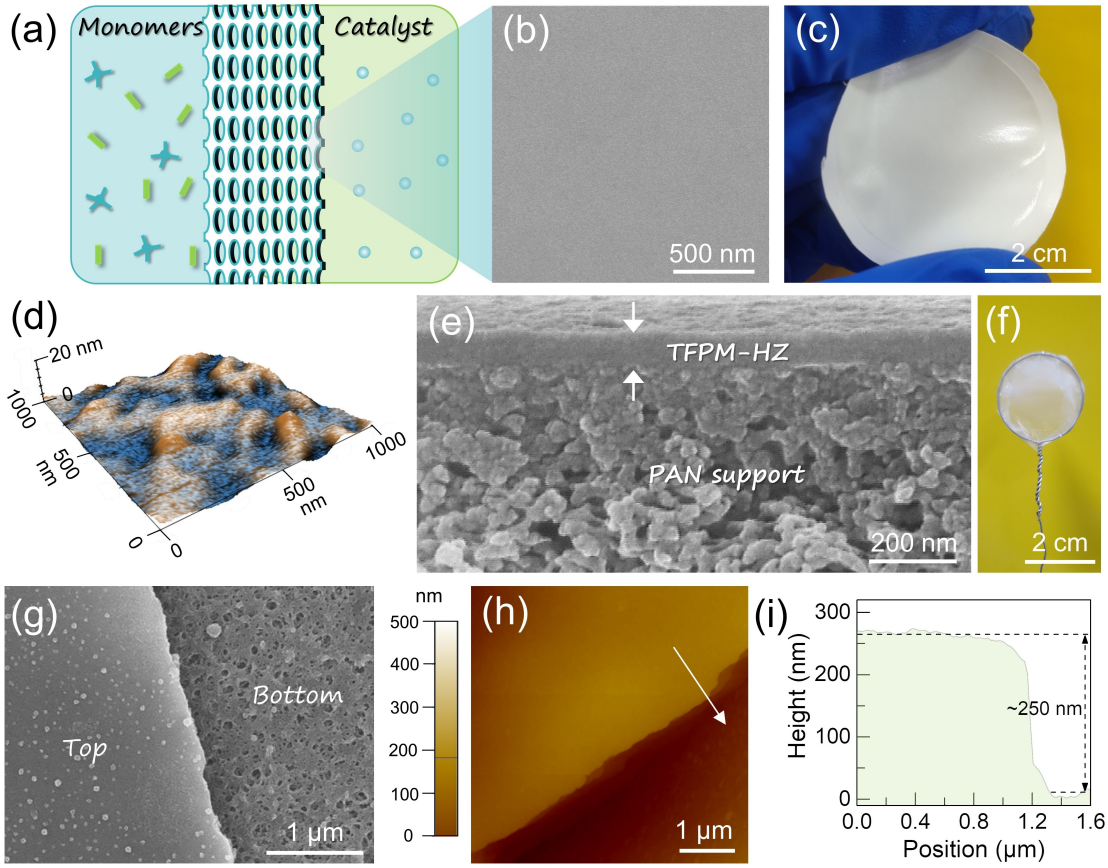

Figure 2. Preparation and characterization of TFPM-HZ/PAN membranes. a) Schematic illustration of the membrane synthesis. b–e) Surface SEM, digital, AFM, and cross-sectional SEM images of the membrane. f) Photograph of the s-TFPM-HZ membrane supported on a metal lasso. g–i) SEM, AFM images, and height profile of the s-TFPM-HZ membrane. Height profile in (i) is along with the arrow shown in (h).

composite membranes prepared by transferring methods.[29] Moreover, ultrasonic treatments cause negligible damages to the membrane integrality (Figure S15), highlighting its robustness to resist harsh operational conditions. The developed synthetic method additionally holds a favorable universality, which allows the production of other COF membranes (Figure S16).

To understand the chemical composition of the TFPM-HZ/PAN membrane, we performed FTIR and X-ray photoelectron spectroscopy (XPS) characterizations. Upon the TFPM-HZ growth, a new stretching vibration emerging at 1624 cm^{-1} refers to the imine linkage, in line with the XPS result (Figure 3a, Figure S17). The consistency of TGA results between the s-TFPM-HZ membrane and the solvothermally synthesized powder indicates the high purity (no PAN) and thermal stability of these detached membranes (Figure S18). The PXRD pattern recorded on the s-TFPM-HZ membrane shows a notable peak at 2θ of 9.4° (Figure 3b), revealing the strong crystallinity. We conducted the high-resolution TEM (HRTEM) characterization on the s-TFPM-HZ membrane synthesized for 36 h. Consistent with the XPS analysis, the s-TFPM-HZ membrane presents the signals of C and N elements (Figure 3c). Significantly, the lattice fringes observed in the HRTEM image confirm the crystalline architecture of the interfacially synthesized TFPM-HZ (Figure 3d).[30] The surface properties of TFPM-HZ/PAN membranes were investigated to correlate the characteristic and performance. Zeta potential tests were used to evaluate the surface charges as a function of pH values. Due to the neutral framework of TFPM-HZ, the resultant membrane exhibits neutralized surface charge intensity (Figure 3e). Following this, we studied the wettability of TFPM-HZ and PAN membranes toward water and methanol. As shown in Figure 3f, the PAN support shows a hydrophilic surface with a water contact angle of ≈68°, while the hydrophilicity largely decreases for the composite membrane. We ascribe this to the structural specificity of TFPM-HZ, of which the hydrophobic phenyl ring is largely involved. Interestingly, the TFPM-HZ/PAN membrane delivers an extremely high affinity to methanol despite its angstrom-level channels, affording fast penetration of methanol within 2 s (Figure 3g). However, water droplet barely permeates into the membrane, which is essentially identical to the hydrophobic skeleton (Figure S19). Thus, the sub-nanometer pore and favorable organic solvent penetration empower the potential application of our membranes in high-performance OSN.

OSN performances of the TFPM-HZ/PAN membrane synthesized for 48 h were investigated by dead-end filtration with a trans-membrane pressure of 1 bar. Figure 4a depicts

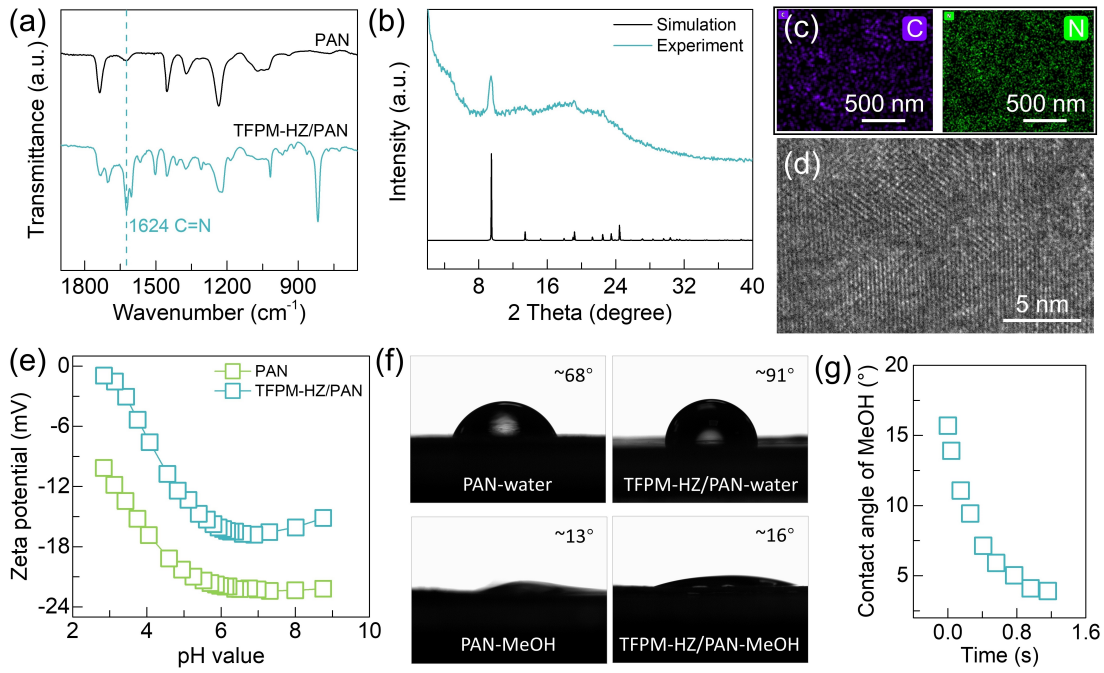

Figure 3. Structure and property characterizations of TFPM-HZ/PAN membranes. a) FTIR spectra of the support and membrane. b) Experimental and simulated PXRD patterns of s-TFPM-HZ membranes. c,d) Surface elemental mapping and HRTEM images of the s-TFPM-HZ membrane. e,f) Zeta potential curves and solvent contact angles of the support and membrane. g) Change of the methanol (MeOH) contact angle with time. Dash line in (a) indicates the position of the characteristic peak.

the permeances of water as well as a variety of organic solvents. In the light of the 3D interconnected porosity,[31] the TFPM-HZ/PAN membrane delivers prominent permeances to the majority of tested solvents. Notably, in spite of its larger kinetic diameter, methanol exhibits a remarkable permeance of $\approx 44\ L\,m^{-2}\,h^{-1}\,bar^{-1}$, which is four times higher than water permeance. The hydrophobic architecture of TFPM-HZ rationalizes this, as the surface hydrophobicity impedes water permeation while allowing the accelerated transport of methanol,[32] in consistence with the above wettability result. The solvent permeance value is primarily dominated by the viscosity of solvents. Consistent with previously reported works,[33] the observed domination can be exemplified by the Hagen-Poiseuille equation, which illustrates an inverse correlation between solvent viscosity and permeance. However, the solvent permeance across the membrane presents a nonlinear relationship with the reciprocal of solvent viscosity. This mainly arises from the molecular interactions between solvents and TFPM-HZ pore walls, in agreement with the modeling study.[34]

Considering that methanol ranks top five solvents in pharmaceutical industry,[1] we targeted it as the representative organic solvent for the following investigation. The methanol permeance is found to be linearly proportional to the applied pressure, showing a constant flux under high pressures (Figure 4b). This corresponds to the excellent mechanical strength of our membranes. We evaluated the membrane selectivity by filtrating methanolic solutions which contain various probe dyes with molecular weights ranging from ≈ 287 to ≈ 961 Da (Figure S20). The membrane exhibits exceptional separation performances to these small molecules, attaining remarkable rejection rates of $>95\,\%$ to probes with molecular weights over 327 Da (Figure 4c, Figure S21). Our membrane also reaches an 83 % rejection to mordant orange 1 (MO-1, $M_w = 287$ Da) with a high permeance, indicative of its capability of separating low-molecular-weight targets. In additional, an incremental rejection against the molecular weight is observed, revealing the size-dependent selectivity across the rigid channels of TFPM-HZ. Evaluating the rejection profile recognizes a nominal molecular weight cut-off (MWCO) of ≈ 300 Da in methanol. This appealing MWCO value mostly originates from the ordered channels with an ultrafine aperture in TPFM-HZ, which are capable of effectively rejecting molecules by pore-size exclusion. Of note, under an analogous molecular selectivity, the methanol permeability (permeance × thickness) of the TFPM-HZ/PAN membrane is about 28-fold as much as the value offered by the unactivated 8-nm-thick PA membrane.[28] This highlights the exceptional advantage of the crystalline membrane over amorphous polymeric ones. In the filtration, of particular interest is the invariant permeation flux toward different feeding solutions, which is close to the pure methanol flux as indicated by the gray line in Figure 4c. Due to the suboptimal pore uniformity and structural instability, the solute molecules could easily penetrate into the separation layers and even supports to block the initial channels under trans-membrane pressures.[2] This leads to impeded pathways and therefore declined fluxes during separation, which is frequently observed in traditional OSN processes.[7b] In sharp contrast to the dyed PAN support after filtration, the growth of a thin TFPM-HZ layer thoroughly prevents the

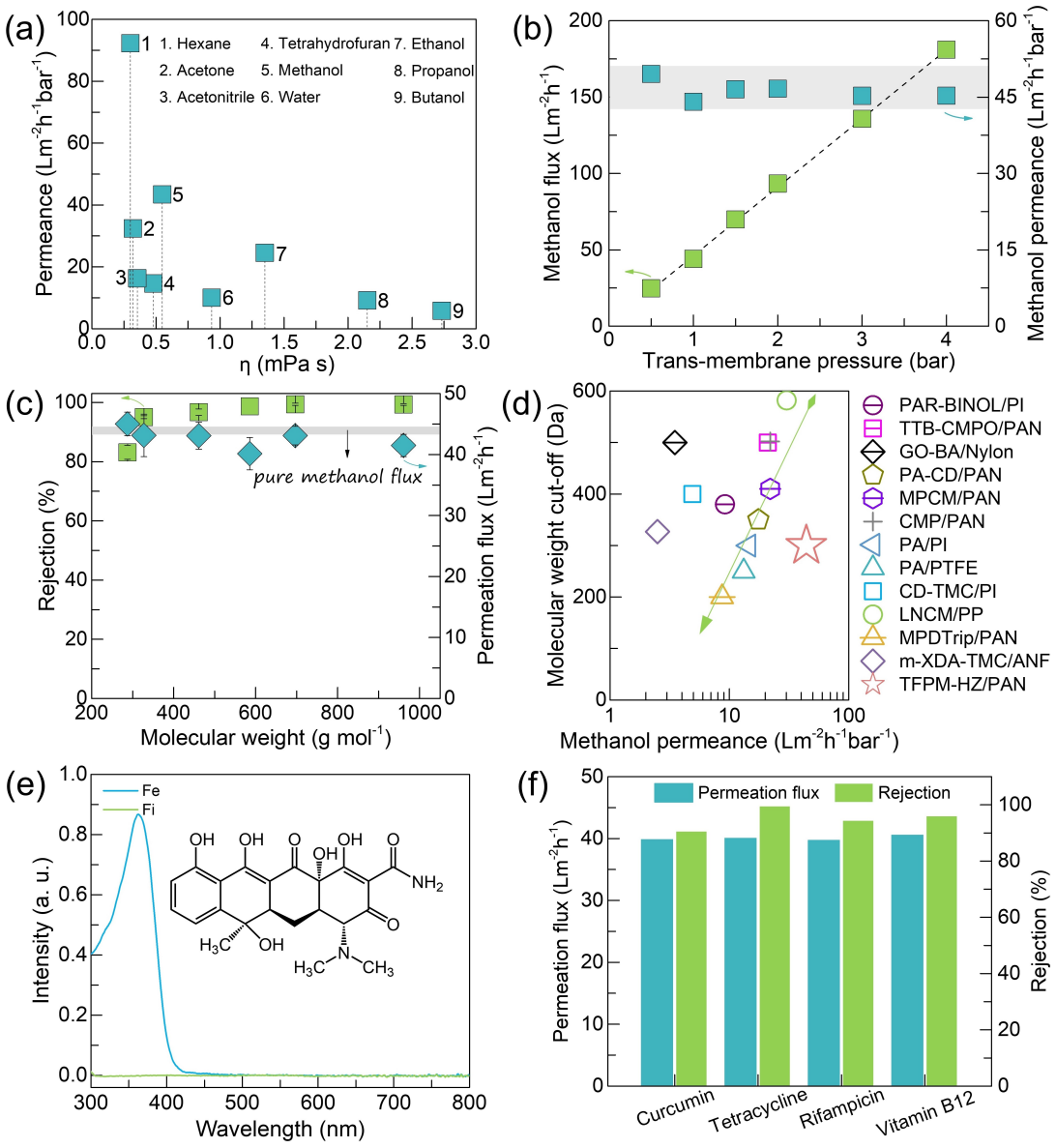

Figure 4. OSN performances of the TFPM-HZ/PAN membrane. a) Pure solvent permeance as a function of viscosity. b) Methanol flux and permeance versus applied pressures. c) Rejection and methanol flux when filtrating solutions containing diverse molecules. d) Comparison of OSN performances between our membrane and others. e) UV-Vis absorption spectra of the methanolic tetracycline solution before and after filtration. f) Rejection and methanol flux when filtrating API solutions. Inset in (e) shows the molecular structure of tetracycline.

solute penetration (Figure S22), thus keeping the filtration flux nearly unchanged. The smooth membrane surface with no rugged areas to capture solutes partly benefits the stabilization of flux as well. The remarkably retained flux could improve productivity and reduce energy consumption, promising cost-efficient OSN operations. To present an intuitive demonstration of the membrane superiority, we provided a comparison of our membranes with the state-of-the-art membranes built of competent materials, such as graphene oxide, PA and derivatives, and porous polymers (Figure 4d, Table S1). As indicated by the arrow, lowering the MWCO value requires a large sacrifice in solvent permeance, which shows a serious selectivity-permeability trade-off. On the contrary, our membrane not only attains a sharp selectivity, but also presents an unprecedentedly high permeance that is 2–10 times higher than those reported in literature. These results reveal the excellence of TFPM-HZ in building OSN membranes with record performances. In terms of water treatment, the membrane yields a decent ion separation performance with a sodium sulfate rejection of ≈63.5 %, suggesting the possibility of 3D COFs for desalination and ion separation.

Motivated by excellent OSN performances, we sought to investigate the applicability of the synthesized membrane in pharmaceutical industry.[35] To demonstrate the competence of our membranes in treating a wide range of pharmaceutical scopes, important APIs with diverse functions and structures are selected to implement separations. According

to the spectral results, these APIs can be effectively rejected by the TFPM-HZ/PAN membrane (Figure 4e, Figure S23). In detail, the membrane exhibits a rejection rate of ≈91 %, ≈100 %, ≈95 %, and ≈96 % for curcumin, tetracycline, rifampicin, and vitamin B12, respectively (Figure 4f). Similarly, the methanol permeation flux is primarily maintained when filtrating these API solutions. We should note that, unlike routine reports which only assess OSN performances by rejecting dyes, this work consciously presents the usability of the TFPM-HZ/PAN membrane for practical separation of high-value pharmaceutical molecules. It validates that the membrane precisely engineered by TFPM-HZ can be an ideal candidate widely suitable for pharmaceutical industries.

A persistent obstacle of OSN membranes is their potential instability in organic solvents, which could pose structural damage and performance deterioration in consecutive runs.[8] In this study, we envision a desirable robustness of our membranes by exerting the highly crystallized skeleton of TFPM-HZ. As expected, no physical cleavage or chemical decomposition can be observed for the s-TFPM-HZ membrane after being soaked in polar and nonpolar solvents for 3 weeks (Figure S24). Moreover, the immersion of the membrane in DMF for 5 months negligibly changes the appearance and structure (Figure 5a), implying a strong solvent resistance. Highly concentrated feeds in industrial implementation are prone to arouse considerable concentration polarization at the membrane surface, which is detrimental to permselectivity.[2] To visualize the stability against high-concentration feeds, we performed separation tests by filtrating methanolic rifampicin solutions with increased concentrations in the range of 50–500 ppm. Figure 5b presents the appearance variation of the feed from orange to colorless when processing the 200-ppm rifampicin solution through the TFPM-HZ/PAN membrane, indicating a steady selectivity regardless of high concentrations. The filtration tests reveal a highly stable separation ability of our membranes to these high-concentration pharmaceutical feeds, which still receive compelling rejections above 90 % (Figure 5c, Figure S25). These results suggest that the membrane is particularly suitable and competitive for processing concentrated solutions. Compared with low-concentration feeds, the methanol flux presents a slight decrease, which is the result of the increased osmotic pressure and additional mass transport resistance.[36] The performance durability is of profound significance from industrial perspectives. Thus, the long-term filtration test was conducted to validate the durability of the TFPM-HZ/PAN membrane. As illustrated in Figure 5d, both methanol flux and acid fuchsin (AF) rejection are unexpectedly

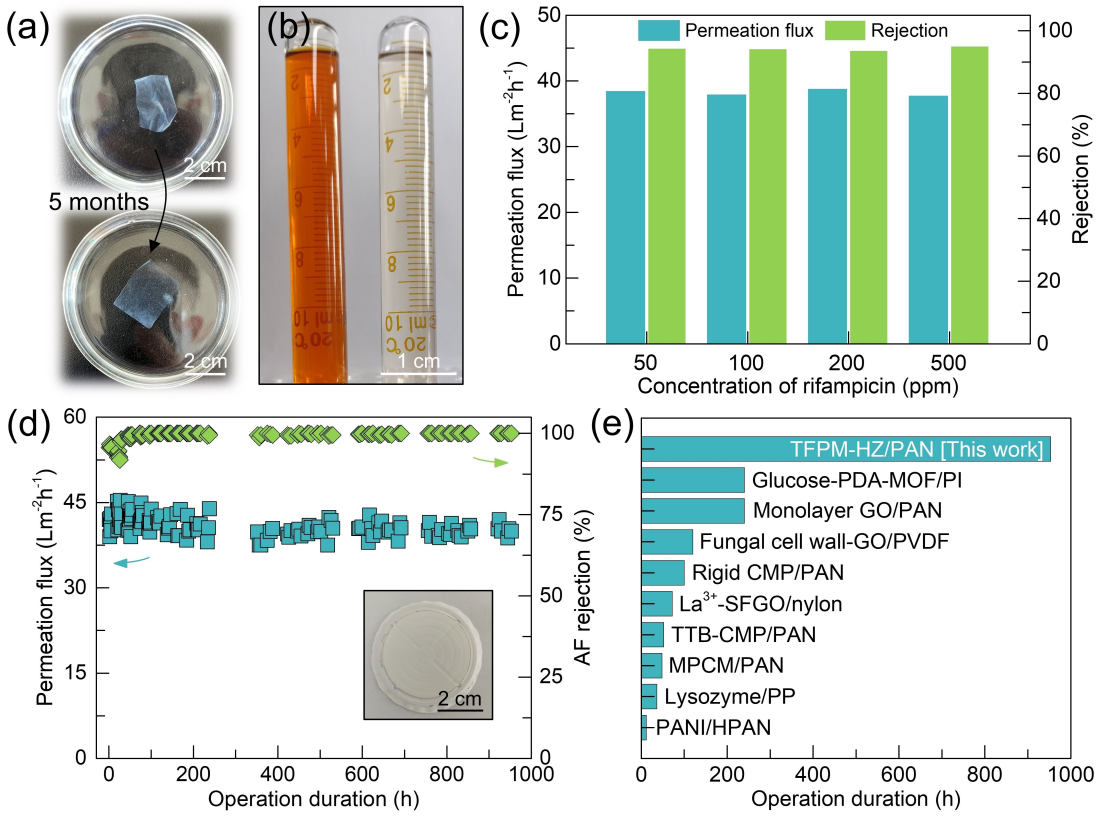

Figure 5. Stability and durability evaluations of the TFPM-HZ/PAN membrane. a) Photographs of the s-TFPM-HZ membrane immersed in DMF for 5 months. b) Photograph showing the 200-ppm methanolic rifampicin solution before (left) and after (right) filtration. c) Methanol flux and rejection rate when filtrating the methanolic rifampicin solutions with various concentrations. d) Performance change under a long-term filtration at the pressure of 1 bar. e) Comparison of the operational duration between our membrane and others. Inset in (d) is the photograph of the membrane after the long-term filtration.

maintained in about 1000-h continuous filtration. Moreover, the membrane subjected to this prolonged separation keeps intact without any damages or fouling (inset in Figure 5d). These demonstrate that the TFPM-HZ/PAN membrane experiences inappreciable physical aging, compaction, or swelling issues, and the separation layer tightly attaches to the support without detachment. Different from those membranes facing the problems of swelling and poor bonding forces, the crystalline TFPM-HZ/PAN membrane substantially tackles the above limitations, free of tedious pre-synthetic and post-synthetic modifications. We also summarized typical results in the recent studies reporting the operational stability of OSN membranes and diagrammatized the operation duration in Figure 5e. It should be noted that the performance deteriorates for most of these membranes in spite of short operation durations (Table S2). In the present work, the stably operated duration of the TFPM-HZ/PAN membrane greatly exceeds other membranes,[37] providing impressive practicality over its analogues. Therefore, the reliability in the aspect of structure and performance proves the merits of TFPM-HZ in building powerful OSN membranes toward real-world applications.

Conclusion

In summary, we demonstrate unprecedentedly stable and highly permselective OSN membranes, derived from the structural design of organic frameworks in terms of aperture size and dimensional connectivity. Nanoporous supports realize the controlled release of catalysts to interfacially crystalize membranes with an extremely robust structure. The established 3D COF platform conquers the key bottlenecks of OSN membranes by exerting its unique merits including rigid crystalline frameworks, spatially continuous channels, and hydrophobic pore chemistry. As a result, the TFPM-HZ/PAN membrane receives an exceptional solvent permeance and high molecular selectivity, which largely surpass state-of-the-art OSN membranes. Significantly, the uniform and non-deformable skeleton arising from the crystalline nature produces record durability against solvent swelling and physical aging, allowing a month-long operation. These distinctive characteristics make our membrane particularly feasible for purifying diverse bioactive molecules, illustrating a wide practicality in pharmaceutical industries. This work offers a design principle for synthesizing crystalline polymeric membranes, and the developed 3D COF membrane promises extensive applications desiderating energy-efficient nanofiltration.

Author Contributions

The manuscript was written through contributions of all authors. All authors have given approval to the final version of the manuscript.

Acknowledgements

This work was supported by the National Natural Science Foundation of China (21825803, 22008110). X. S. also thanks the China Postdoctoral Science Foundation (2022 T150318) for support.

Conflict of Interest

The authors declare no conflict of interest.

Data Availability Statement

The data that support the findings of this study are available in the supplementary material of this article.

Keywords: Active Pharmaceutical Ingredients · Covalent Organic Frameworks · Molecular Separation · Organic Solvent Nanofiltration · Structural Design

[1] D. J. C. Constable, C. Jimenez-Gonzalez, R. K. Henderson, *Org. Process Res. Dev.* **2007**, *11*, 133–137.
[2] L. Nie, C. Y. Chuah, T. H. Bae, J. M. Lee, *Adv. Funct. Mater.* **2021**, *31*, 2006949.
[3] C. J. Clarke, W. C. Tu, O. Levers, A. Brohl, J. P. Hallett, *Chem. Rev.* **2018**, *118*, 747–800.
[4] P. Vandezande, L. E. Gevers, I. F. Vankelecom, *Chem. Soc. Rev.* **2008**, *37*, 365–405.
[5] D. S. Sholl, R. P. Lively, *Nature* **2016**, *532*, 435–437.
[6] B. Liang, X. He, J. Hou, L. Li, Z. Tang, *Adv. Mater.* **2019**, *31*, 1806090.
[7] a) Y. Lu, L. Zhang, L. Shen, W. Liu, R. Karnik, S. Zhang, *Proc. Natl. Acad. Sci. USA* **2021**, *118*, e2111360118 ; b) Y. Li, E. Wong, A. Volodine, C. Van Haesendonck, K. Zhang, B. Van der Bruggen, *J. Mater. Chem. A* **2019**, *7*, 19269–19279; c) W. Wei, K. M. Gupta, J. Liu, J. W. Jiang, *ACS Appl. Mater. Interfaces* **2018**, *10*, 33135–33143.
[8] P. Marchetti, M. F. Jimenez Solomon, G. Szekely, A. G. Livingston, *Chem. Rev.* **2014**, *114*, 10735–10806.
[9] S. Y. Zhou, Y. L. Zhao, J. F. Zheng, S. B. Zhang, *J. Membr. Sci.* **2019**, *591*, 117347.
[10] B. Liang, H. Wang, X. H. Shi, B. Y. Shen, X. He, Z. A. Ghazi, N. A. Khan, H. Sin, A. M. Khattak, L. S. Li, Z. Y. Tang, *Nat. Chem.* **2018**, *10*, 961–967.
[11] a) Q. Yang, Y. Su, C. Chi, C. T. Cherian, K. Huang, V. G. Kravets, F. C. Wang, J. C. Zhang, A. Pratt, A. N. Grigorenko, F. Guinea, A. K. Geim, R. R. Nair, *Nat. Mater.* **2017**, *16*, 1198–1202; b) C. Chen, J. M. Wang, D. Liu, C. Yang, Y. C. Liu, R. S. Ruoff, W. W. Lei, *Nat. Commun.* **2018**, *9*, 1902.
[12] a) X. He, H. Sin, B. Liang, Z. A. Ghazi, A. M. Khattak, N. A. Khan, H. R. Alanagh, L. S. Li, X. Q. Lu, Z. Y. Tang, *Adv. Funct. Mater.* **2019**, *29*, 1900134; b) L. Y. Zhang, M. C. Zhang, G. P. Liu, W. Q. Jin, X. Y. Li, *Adv. Funct. Mater.* **2021**, *31*, 2100110.
[13] a) S. S. Yuan, X. Li, J. Y. Zhu, G. Zhang, P. Van Puyvelde, B. Van der Bruggen, *Chem. Soc. Rev.* **2019**, *48*, 2665–2681; b) H. J. Wang, M. D. Wang, X. Liang, J. Q. Yuan, H. Yang, S. Y. Wang, Y. X. Ren, H. Wu, F. S. Pan, Z. Y. Jiang, *Chem. Soc. Rev.* **2021**, *50*, 5468–5516; c) H. Z. Dou, M. Xu, B. Y. Wang, Z. Zhang, G. B. Wen, Y. Zheng, D. Luo, L. Zhao, A. P.

Yu, L. H. Zhang, Z. Y. Jiang, Z. W. Chen, *Chem. Soc. Rev.* **2021**, *50*, 986–1029.
[14] S. Kandambeth, B. P. Biswal, H. D. Chaudhari, K. C. Rout, H. S. Kunjattu, S. Mitra, S. Karak, A. Das, R. Mukherjee, U. K. Kharul, R. Banerjee, *Adv. Mater.* **2017**, *29*, 1603945.
[15] D. B. Shinde, G. Sheng, X. Li, M. Ostwal, A. H. Emwas, K. W. Huang, Z. P. Lai, *J. Am. Chem. Soc.* **2018**, *140*, 14342–14349.
[16] a) H. W. Fan, A. Mundstock, A. Feldhoff, A. Knebel, J. H. Gu, H. Meng, J. Caro, *J. Am. Chem. Soc.* **2018**, *140*, 10094–10098; b) F. M. Sheng, B. Wu, X. Y. Li, T. T. Xu, M. A. Shehzad, X. X. Wang, L. Ge, H. T. Wang, T. W. Xu, *Adv. Mater.* **2021**, *33*, 2104404; c) Y. Li, Q. X. Wu, X. H. Guo, M. C. Zhang, B. Chen, G. Y. Wei, X. Li, X. F. Li, S. J. Li, L. J. Ma, *Nat. Commun.* **2020**, *11*, 599; d) X. S. Shi, Z. Zhang, S. Y. Fang, J. T. Wang, Y. T. Zhang, Y. Wang, *Nano Lett.* **2021**, *21*, 8355–8362.
[17] X. S. Shi, Z. Zhang, M. J. Wei, X. Y. Wang, J. T. Wang, Y. T. Zhang, Y. Wang, *Macromolecules* **2022**, *55*, 3259–3266.
[18] H. B. Park, J. Kamcev, L. M. Robeson, M. Elimelech, B. D. Freeman, *Science* **2017**, *356*, 1137.
[19] Z. Y. Wang, Z. X. Wang, S. H. Lin, H. L. Jin, S. J. Gao, Y. Z. Zhu, J. Jin, *Nat. Commun.* **2018**, *9*, 2004.
[20] a) H. M. El-Kaderi, J. R. Hunt, J. L. Mendoza-Cortes, A. P. Cote, R. E. Taylor, M. O'Keeffe, O. M. Yaghi, *Science* **2007**, *316*, 268–272; b) S. F. Chen, C. J. Zhu, W. P. Xian, X. Y. Liu, X. L. Liu, Q. H. Zhang, S. Q. Ma, Q. Sun, *J. Am. Chem. Soc.* **2021**, *143*, 9415–9422.
[21] S. J. Rowan, S. J. Cantrill, G. R. L. Cousins, J. K. M. Sanders, J. F. Stoddart, *Angew. Chem. Int. Ed.* **2002**, *41*, 898–952.
[22] S. Kandambeth, V. Venkatesh, D. B. Shinde, S. Kumari, A. Halder, S. Verma, R. Banerjee, *Nat. Commun.* **2015**, *6*, 6786.
[23] H. L. Nguyen, C. Gropp, N. Hanikel, A. Möckel, A. Lund, O. M. Yaghi, *ACS Cent. Sci.* **2022**, https://doi.org/10.1021/acscentsci.2c00398.
[24] X. Y. Guan, Y. C. Ma, H. Li, Y. Yusran, M. Xue, Q. R. Fang, Y. S. Yan, V. Valtchev, S. L. Qiu, *J. Am. Chem. Soc.* **2018**, *140*, 4494–4498.
[25] X. S. Shi, A. K. Xiao, C. X. Zhang, Y. Wang, *J. Membr. Sci.* **2019**, *576*, 116–122.
[26] a) S. Zhao, C. H. Jiang, J. C. Fan, S. S. Hong, P. Mei, R. X. Yao, Y. L. Liu, S. L. Zhang, H. Li, H. Q. Zhang, C. Sun, Z. B. Guo, P. P. Shao, Y. H. Zhu, J. W. Zhang, L. S. Guo, Y. H. Ma, J. Q. Zhang, X. Feng, F. C. Wang, H. G. Wu, B. Wang, *Nat. Mater.* **2021**, *20*, 1551–1558; b) N. Giuseppone, J. L. Schmitt, E. Schwartz, J. M. Lehn, *J. Am. Chem. Soc.* **2005**, *127*, 5528–5539.
[27] M. Y. Liu, K. Jiang, X. Ding, S. L. Wang, C. X. Zhang, J. Liu, Z. Zhan, G. Cheng, B. Y. Li, H. Chen, S. B. Jin, B. Tan, *Adv. Mater.* **2019**, *31*, 1807865.
[28] S. Karan, Z. W. Jiang, A. G. Livingston, *Science* **2015**, *348*, 1347–1351.
[29] D. B. Shinde, L. Cao, A. D. D. Wonanke, X. Li, S. Kumar, X. Liu, M. N. Hedhili, A. H. Emwas, M. Addicoat, K. W. Huang, Z. P. Lai, *Chem. Sci.* **2020**, *11*, 5434–5440.
[30] C. Y. Fan, H. B. Geng, H. Wu, Q. Peng, X. Y. Wang, B. B. Shi, Y. Kong, Z. Y. Yin, Y. Q. Liu, Z. Y. Jiang, *J. Mater. Chem. A* **2021**, *9*, 17720–17723.
[31] A. He, Z. Jiang, Y. Wu, H. Hussain, J. Rawle, M. E. Briggs, M. A. Little, A. G. Livingston, A. I. Cooper, *Nat. Mater.* **2022**, *21*, 463–470.
[32] S. Karan, S. Samitsu, X. S. Peng, K. Kurashima, I. Ichinose, *Science* **2012**, *335*, 444–447.
[33] L. Nie, K. Goh, Y. Wang, J. Lee, Y. J. Huang, H. E. Karahan, K. Zhou, M. D. Guiver, T. H. Bae, *Sci. Adv.* **2020**, *6*, eaaz9184.
[34] P. H. H. Duong, Y. K. Shin, V. A. Kuehl, M. M. Afroz, J. O. Hoberg, B. Parkinson, A. C. T. van Duin, K. D. Li-Oakey, *ACS Appl. Mater. Interfaces* **2021**, *13*, 42164–42175.
[35] M. G. Buonomenna, J. Bae, *Sep. Purif. Rev.* **2015**, *44*, 157–182.
[36] L. Shen, Q. Shi, S. P. Zhang, J. Gao, D. C. Cheng, M. Yi, R. Y. Song, L. D. Wang, J. W. Jiang, R. Karnik, S. Zhang, *Sci. Adv.* **2021**, *7*, eabg6263.
[37] T. F. Huang, T. Puspasari, S. P. Nunes, K. V. Peinemann, *Adv. Funct. Mater.* **2020**, *30*, 1906797.

Manuscript received: May 23, 2022
Accepted manuscript online: July 16, 2022
Version of record online: July 28, 2022